

Characterization of a GaAs Medipix3 X-ray detector

September 7, 2012



Hugo Dacasa Pereira, Universidade de Vigo.

Anna Grassi, Università di Pisa.

Supervisors: David Pennicard, Julian Becker.

Abstract

The performance of a GaAs Medipix3 hybrid pixel detector is tested in this work. Its two main operation modes (single pixel mode and charge summing mode) are tested and compared, in order to know its optimal working settings, such as bias voltage or threshold values.

For this purpose, images are taken and threshold scans performed. The response of both the whole detector and individual pixels is analyzed. Imaging and spectroscopic properties of the detector are shown. In the case of imaging, the GaAs Medipix3 chip is compared to two different Si Medipix2 chips. Also, the imaging response for hard X-rays is tested for the GaAs.

Contents

1	Introduction	3
1.1	The GaAs Medipix3 detector	3
1.2	The Pixelman software	6
1.3	The X-ray source	6
2	GaAs tests	7
2.1	Current-voltage characteristics	7
2.2	Single pixel mode (SPM)	8
2.2.1	Flat image analysis	8
2.2.2	Repeated threshold scans for a fixed bias voltage	10
2.2.3	Analysis for individual pixels	11
2.2.4	Response to different voltages	12
2.2.5	Flat images with different voltages	14
2.3	Charge summing mode (CSM)	15
2.3.1	Flat images	15
2.3.2	Response to different voltages	16
2.3.3	Analysis for individual pixels	18
2.3.4	Absorption Spectrum	19
3	Imaging	20
3.1	Si Medipix2 chip, 300 μm width	21
3.2	Si Medipix2 chip, 500 μm width	22
3.3	GaAs Medipix3 chip	23
4	Conclusions	27

1 Introduction

Medipix is a hybrid pixel detector readout chip developed by an international collaboration, hosted by CERN.

The hybrid pixel detector technology was initially developed for particle physics detectors, but the Medipix chip has shown that the technology is also good for X-ray imaging and spectroscopy.

Unlike CCD (charged-coupled device) detectors, which operate exclusively on an integral basis (that is, a charge is accumulated during exposure and measured afterwards), this detector allows for single photon counting, and obtaining information about the incident radiation's spectrum. Furthermore, its readout system consists of an independent circuit for each single pixel, rendering it extremely fast, but with a drawback: there are differences in the sensitivities of its pixels, which make an equalization procedure necessary.

The Medipix detector family has been in development since the 1990's, and is currently on its third generation. All three generations are compared in table 1.

Generation	Pixel size	Transistors per pixel	CMOS technology	Resolution
Medipix1	170 μm	400	1 μm	64 \times 64
Medipix2	55 μm	500	0.25 μm	256 \times 256
Medipix3	55 μm	1600	0.13 μm	256 \times 256

Table 1: Medipix chip characteristics. [2]

Another important improvement on Medipix3 is the new charge summing mode (CSM), which makes it possible to compensate for the charge sharing effect via inter-pixel communication, optimizing the photon counting process and spectroscopic information obtained.

Most of these detectors are currently based on silicon photodiodes, which can be reliably produced with good uniformity. The problem is that they are not useful for hard X-ray experiments, as the silicon becomes transparent for high energy photons. That is why it is of major importance to develop detectors made with different materials. In this case, a GaAs(Cr) detector is studied.

1.1 The GaAs Medipix3 detector

The silicon sensor has a 2D array of p-n junctions, normally using p-type implants in lightly-doped n-type silicon, as shown in Fig.1.

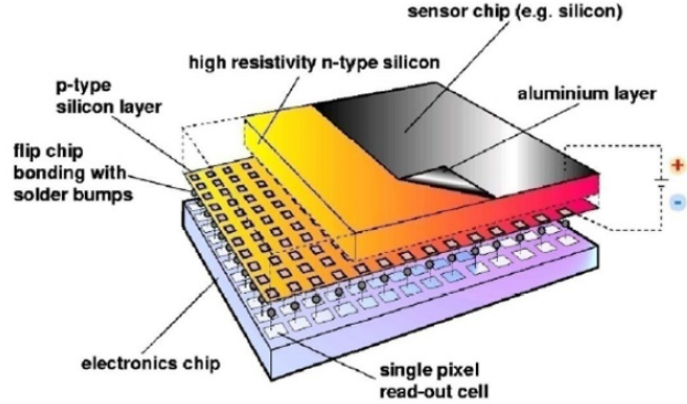


Figure 1: Structure of a silicon Medipix detector

Applying a reverse voltage creates a depletion region where there are few free electrons and holes. This means that it is possible to create a strong electric field inside the silicon, without producing a large flow of current.

To optimize readout speed, each single pixel is bump-bonded to its own readout circuitry, which is part of the Medipix3 chip. These junctions can act as photodiodes if correctly polarized.

The array is made of 256×256 square pixels, of $55 \mu\text{m}$ side. The chip used for this work is composed of a doped GaAs bulk.

The Cr-compensated GaAs sensor does not have p-n junctions, but it naturally has very few free electrons and holes present. So, it is possible to use it as a photoresistor. Applying a large voltage to the sensor creates a strong electric field inside the sensor, without producing a very large current. When a photon transfers its energy to the semiconductor bulk, an electron-hole pair is generated, and these charge carriers are accelerated by the intense electric field present in the depletion region, expanded by the reverse bias voltage; then, a voltage pulse can be measured by the pixels' circuitry. Each pulse is the result of a single photon hit, and its amplitude is proportional to the photon energy. This way, single photons can be counted and their energies measured.

Each analog signal is then processed in the pixel's readout circuit by a preamplifier, then a shaper, and then passed to a comparator. This allows the pixel to detect whenever a signal pulse occurs, and increment a counter in the pixel. However, if two photons, hit the same pixel within a short time period, the chip might not distinguish the second pulse from the first one. The minimum time period between hits to allow them to be correctly read is called dead time. Several parameters can be changed by means of DAC (digital to analog converter) circuitry. One of those parameters is the energy threshold. An interesting feature of the Medipix chips is that both a low and high threshold (THL and THH) can be set, allowing the chip to count photons within a particular energy window if desired, as shown in Fig. 2. Also, Medipix3 features two different counters per pixel, so photons can be counted, for example, both with their energies inside a window and higher than a THL at the same time.

With very low THL, a high amount of noise is detected, as will be shown later.

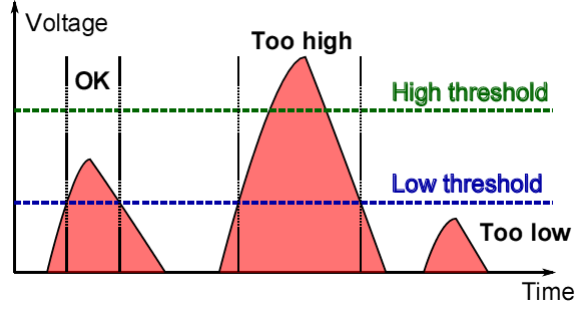


Figure 2: Response to pulses when an energy window is configured. Only the first pulse is detected as a hit. [4]

The chip has two different operation modes in terms of inter-pixel communication, which are the following:

- Single pixel mode (SPM): In this mode, there is no communication between pixels, each one of them is read independently, so there is a charge sharing effect.
- Charge summing mode (CSM): This mode allows for inter-pixel communication, which in turn allows the charge sharing effects to be corrected. As shown in Fig.3 , the charge detected in adjacent pixels is summed in the “summing nodes” placed at the corners of the pixels, which are responsible for the assignment of the hit only to the one with higher signal. This can raise problems if a charge cloud is within one single pixel. To solve this, arbitration circuitry is used to measure which node’s signal remains above the threshold for longest.

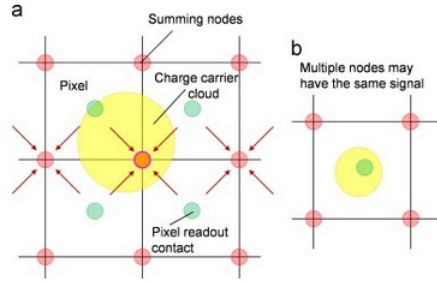


Figure 3: Sketch of charge summing processes. [1]

Data taken in both modes will be analyzed later in detail, showing their pros and cons.

- Spectroscopic mode can be used for both SPM and CSM, which, instead of using normal $55\mu m$ pixels, operates with four-pixel clusters. This way, the circuitry for all four pixels can be combined, making it possible to use 8 threshold levels per cluster, by compromising the spatial resolution, as the clusters are $110\mu m$ in side. This mode allows colour X-ray images to be taken, which permits information about the composition of a sample to be shown within one single picture.

Also, two different gain modes can be set [2]:

- High-gain mode (HG): linearity is reduced but noise is improved.

- Low-gain mode (LG): opposite.

For this work, only high-gain mode is used.

Charge sharing effect may also occur. It is a direct consequence of the charge diffusion inside the semiconductor bulk; a single photon hit might generate a charge carrier cloud that reaches more than one pixel, as shown in Fig.3. This can result in a single photon counted once in each of those affected pixels, and also a lower energy measurement, possibly resulting in some pulses being lower than the THL and therefore, undetected photons.

To save and process the data obtained from the chip, it is connected to a computer via USB port, through an interface which can also generate the bias voltage by itself. In this case, an external high voltage power source is used.

1.2 The Pixelman software

Pixelman is the name of the software used to control, configure and read the chip. It allows several kinds of DACs scans to be performed. In this work, only low threshold (THL) scans are used. It can also perform threshold equalizations for both SPM and CSM, with different settings.

Since every single pixel has its own readout circuit, and there are differences between them caused by the manufacturing process, a threshold equalization procedure is very important in hybrid pixel detectors to minimize these differences. It has to be performed every time the bias voltage is changed. It takes about 20 minutes in SPM and one hour in CSM, as it also has to work with the summing nodes.

A high number of parameters, such as different thresholds or shaper and preamplifier configuration, can be manually set, but the default values are usually good enough. The only DAC value manually changed in this work will be Threshold0. Some of these parameters are shown in Fig.4

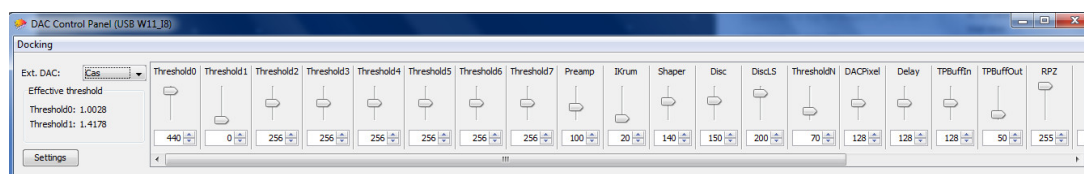


Figure 4: DAC control panel window.

1.3 The X-ray source

The source used for this work was a molybdenum X-ray tube, which radiates a continuous spectrum with a peak around 17.8 keV, the molybdenum fluorescence energy. The voltage that accelerates electrons and the current intensity can both be manually changed. Setting a

higher voltage accounts for a broader energy spectrum. For example, if the voltage is set to 20 kV, the maximum photon energy via bremsstrahlung will be 20 keV, and so on. Additionally, the higher the current intensity, the higher the emitted photon flux, as a consequence of a higher number of electrons being accelerated, but with the same energies. The x-ray tube can be remotely controlled with a computer.

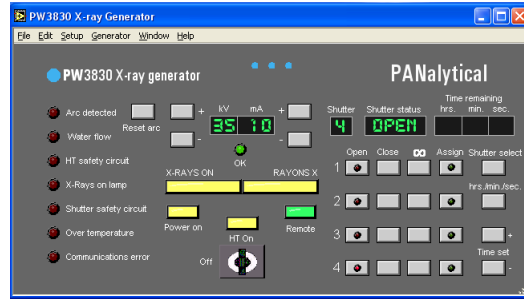


Figure 5: X-ray tube control panel.

2 GaAs tests

2.1 Current-voltage characteristics

First, the detector chip is connected to a power source in reverse bias. The voltage value is changed and the current response measured. The results are shown in Fig. 6.

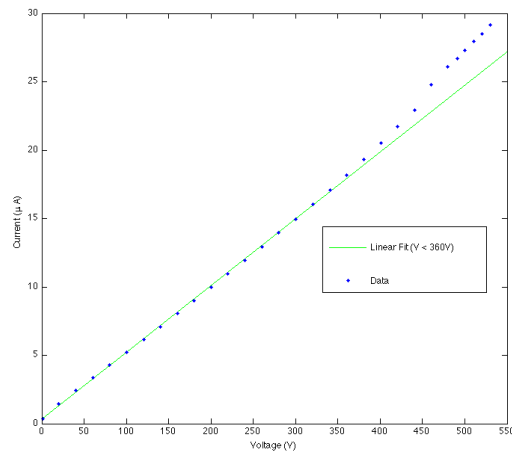


Figure 6: Current versus voltage and linear fit. The linear behaviour is kept with voltages up to 360 V. After that, the slope changes slightly. Because of that, a bias voltage higher than 400 V is never used.

2.2 Single pixel mode (SPM)

2.2.1 Flat image analysis

Before taking any measurements, the bias voltage is set at 300 V and a threshold equalization is performed. After that, the value of the parameter THL0 is set to 35 to leave out part of the noise. Then, a total of 100 flat images are taken with 0.5 s acquisition time. The X-ray tube is set to 35 kV voltage and 10 mA current, and these settings will be kept unless stated otherwise. The images are analyzed afterwards.

As a starting point, an average of the 100 images is calculated. The resulting image is shown in Fig. 7.

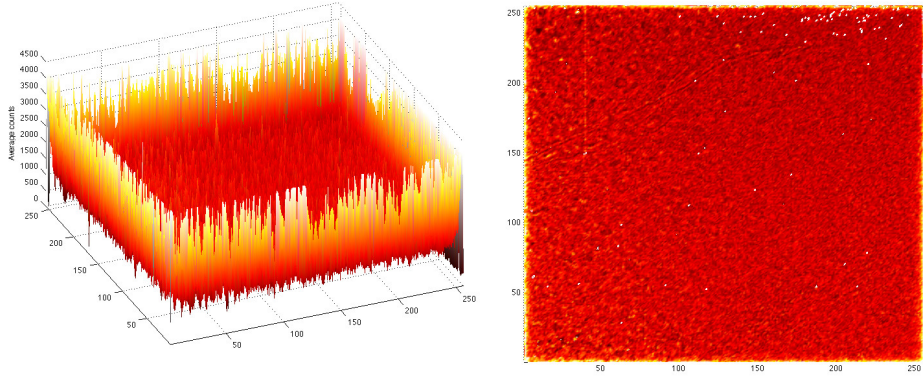


Figure 7: Average flat image from two different angles.

It is obvious that most of the pixels in the edge of the detector are saturated, so it is useful for further analysis to determine what pixels are considered part of the edge. In order to do that, a random line was plotted and smoothed, and it was concluded that the edge was about 12 pixels wide.

A test conducted with the Pixelman software revealed that there are no insensitive pixels with zero counts, however, a straight line of dark pixels can be seen in the upper left part, which will appear in all the images taken with this detector, as well as some other visible structures. The mean value of counts per pixel and the mean value of the standard deviation are

$$m = 1288.6 \quad s = \sqrt{\frac{1}{n-1} \sum_{i=1}^n (x_i - \bar{x})^2} = 35.8 \quad (1)$$

Considering a single pixel, the number of photons from the X-ray tube hitting that pixel will vary from image to image. This variation should follow Poisson statistics. The standard deviation in a single pixel is expected to be the square root of the number of counts provided that the detector does not produce any additional image to image variation. Shown here is the average value of both counts and standard deviation. It shows the pixel behaviour is reasonably stable from image to image.

Poissonian distribution has the property $s^2 = m$. In this case, $s^2 = 1281.3$, which is very close to the calculated mean value. This condition should be met by every single pixel.

The raw histograms are shown in Fig. 8 , and the resulting fits are shown in Fig. 9 and in Table 2.

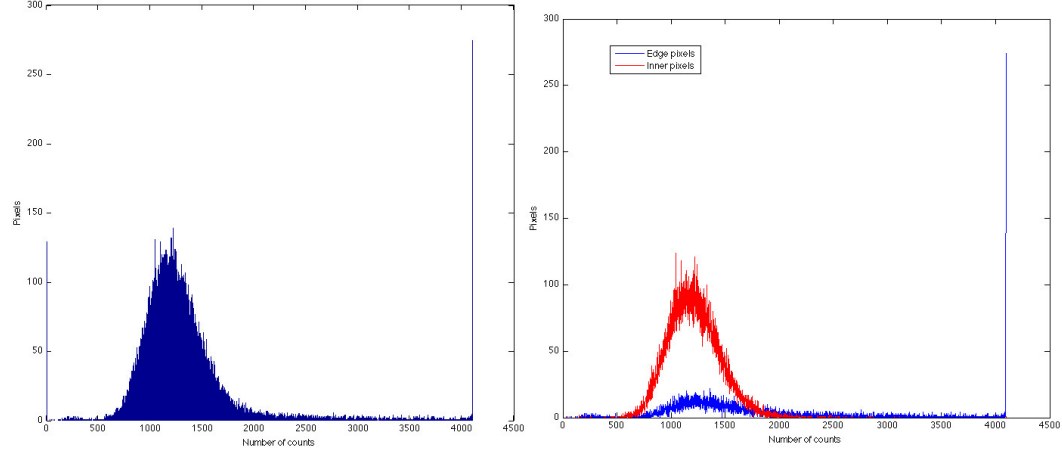


Figure 8: Left: histogram obtained from the average image. Right: comparison between the histogram of the edge pixels (blue) and the inner pixels of (red) of the detector.

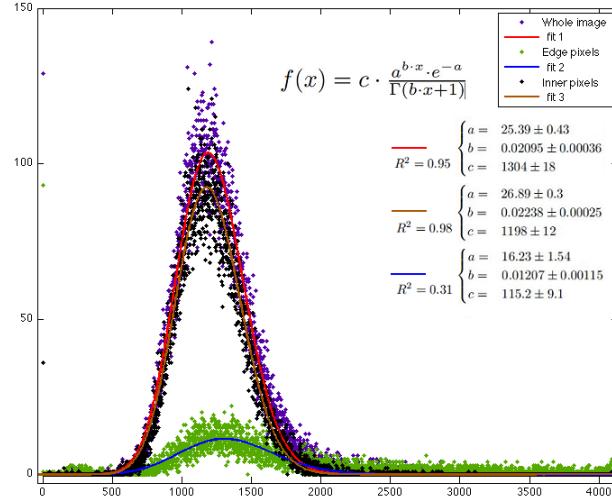


Figure 9: All three histograms and their corresponding fits. The independent variable is continuous, so instead of a factorial, gamma function has to be used. b and c are scale factors. The R squared factor improves when the edge pixels are subtracted.

	Mean value	FWHM	FWHM/mean value
Whole Image	1188	566	0.48
Edge	1303	788	0.60
Center	1179	546	0.46

Table 2: Mean value, FWHM and spread in the three cases. Spread is lower when edge pixels are left out. Also, correlation index is better in that case.

2.2.2 Repeated threshold scans for a fixed bias voltage

The data from different threshold scans is presented and analyzed. It is interesting to analyze first the data obtained within the same voltage setting. The measurements are made for 200 V bias voltage, and repeated ten times to obtain statistical information.

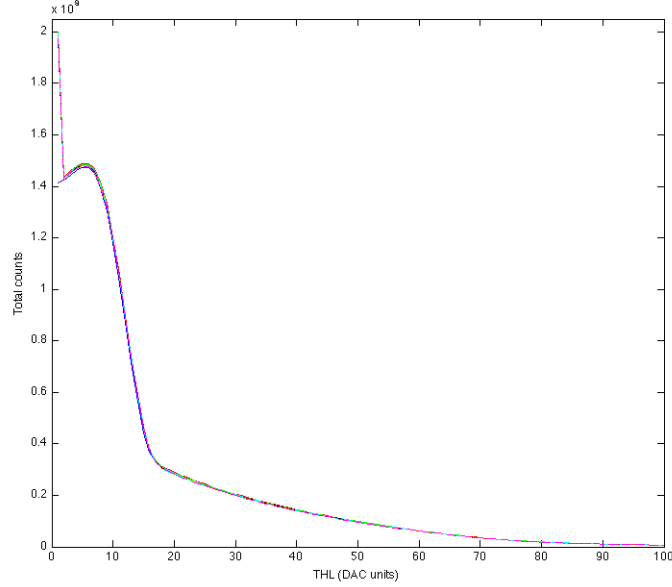


Figure 10: Threshold scan for 200 V bias voltage, repeated 10 times.

The left part of the plots correspond to low threshold settings, so the counts in that region are mostly noise. When the threshold reaches a higher value, the noise level lowers significantly, but not abruptly due to the charge sharing phenomenon.

The inflection point of the lines in Fig.10 (right) represents the molybdenum fluorescence energy, about 18 keV. Because of the voltage setting in the source, the maximum energy of an emitted photon is 35 keV.

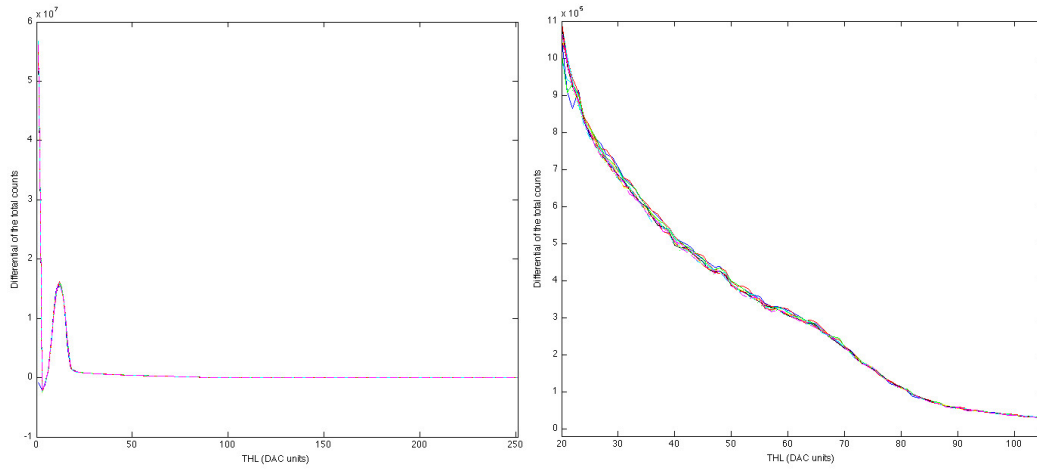


Figure 11: Differential of the previous plot and zoom.

2.2.3 Analysis for individual pixels

The behaviour of some pixels through the threshold scan is detailed next in counts per step. They were randomly selected in some regions of interest, such as the dark line or the edge. The 10 measurements are shown for each pixel in Fig. 12 and Fig. 13.

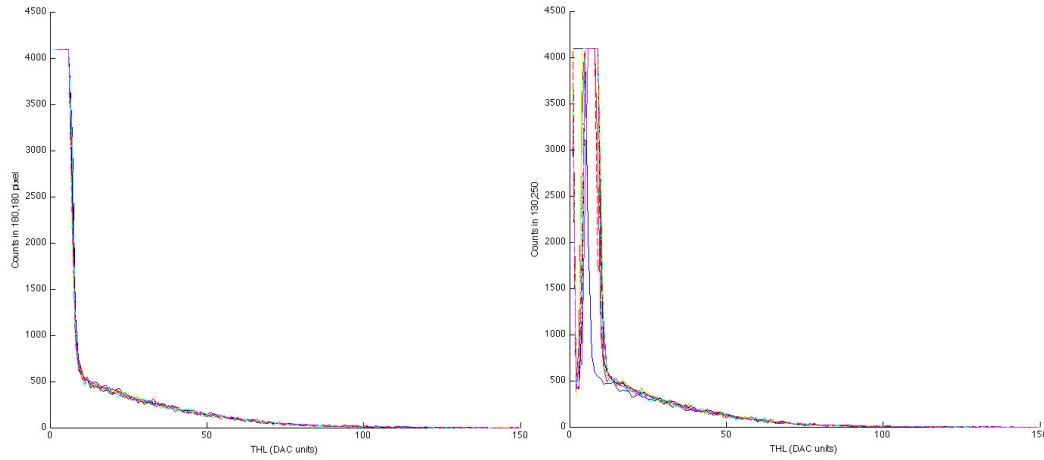


Figure 12: Left: random pixel with an average response which does not fluctuate much over time. Right: pixel from the edge of the detector. Its response changes more over time than a normal pixel, and stays saturated with higher threshold levels.

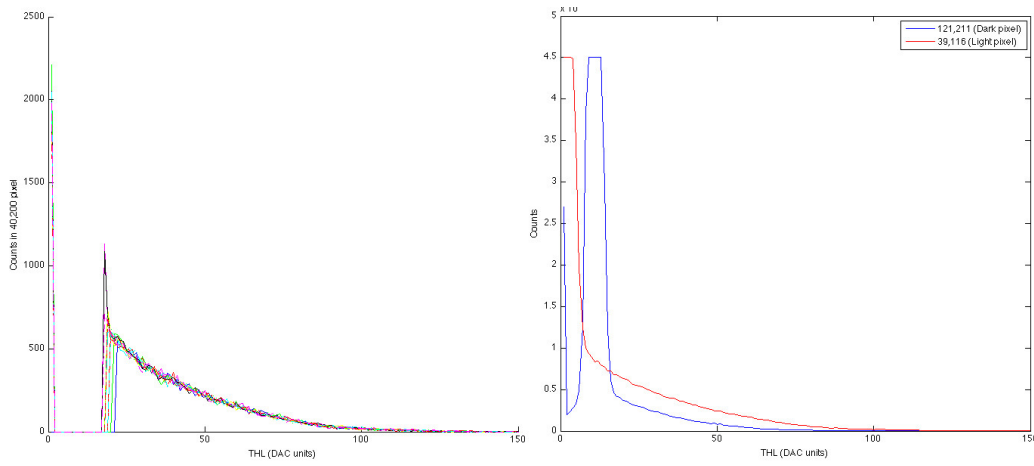


Figure 13: Left: pixel from the aforementioned dark line. No counts seem to be detected under low threshold levels.

Right: comparison between two pixels with different sensitivity.

These trends are the same for every value of bias voltage tested, that is, the edge pixels always detect a high number of counts, and the pixels that make the dark line always detect a low number of counts, and so on.

2.2.4 Response to different voltages

For this part, threshold scans for different bias voltages are analyzed. It is important to perform a threshold equalization every time the voltage is changed.

The applied voltages were between 50 and 400 V.

The data from the threshold scans is shown in Fig.14. The acquisition time was set to $t_{acq} = 0.1$ s, ranging from 0 to 250 DAC units, step 1.

The curves shown in Fig. 14 have the same shape; in the regions of interest, between 30-100 DAC units, the difference in the count numbers can be qualitatively seen. For a more detailed analysis, the differential of these curves is shown in Fig. 15, with a zoom in said region.

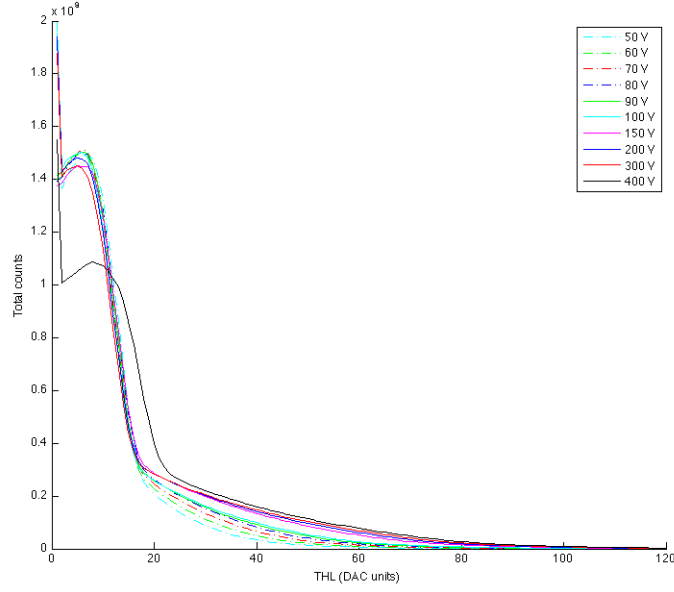


Figure 14: Zoom of the threshold scans for all the bias voltages applied (total counts per step). These are called S-curves. The 400 V curve is too different from the other ones, maybe due to high current through the detector.

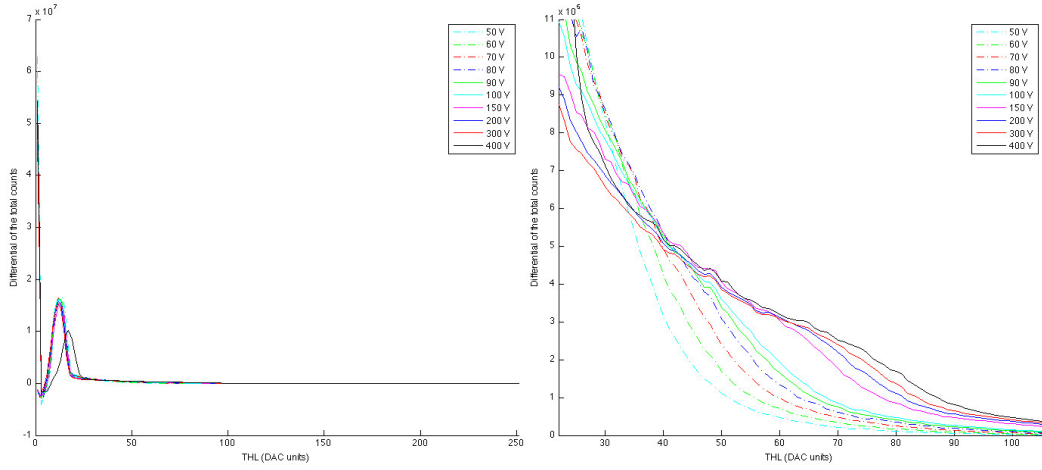


Figure 15: Differential of the previous plots.

For low voltages (lower than 150 V), it is clear that the detector does not show as much information as in other cases. In the plot on the right, it is observed that the molybdenum fluorescence peak is not clearly visible. Besides, the effects of charge sharing seem more

important at low voltages, because the charge generated by the photons hitting the detector take longer to reach the readout chip, so there is more charge diffusion. In that same graph, this is seen as the intersection between the high and low voltage curves. In conclusion, charge sharing makes it difficult to obtain spectroscopic information from these scans.

Another interesting result is that the position of the molybdenum signal moves to lower threshold values as the voltage is reduced. This could be due to charge trapping: at lower voltages, the electrons travel more slowly, so more of them get trapped by defects in the detector and a lower signal is produced.

It is also interesting to study the response of an individual pixel under different bias voltages (Fig. 16). It is clear that the trend in the curve is consistent to the average response shown before in the threshold scans (Fig. 14), that is, the same shape but less sensitivity when low voltages are applied, except for the 400 V case. Also, considering individual pixels, bigger fluctuations of the noisy region's size can be seen, as a consequence of having to perform a threshold equalization for each different voltage.

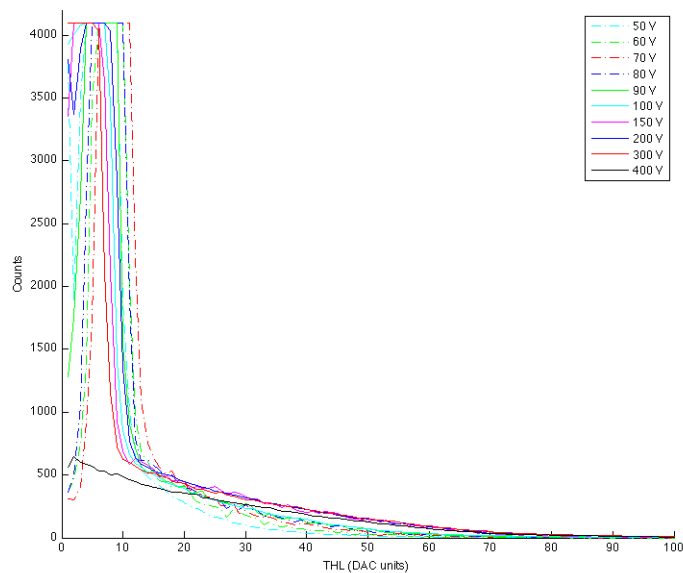


Figure 16: Individual pixel's response to different voltages.

2.2.5 Flat images with different voltages

To conclude the characterization of the detector in SPM, 100 flat images with $t_{acq} = 0.1$ s are taken, changing the bias voltage in the range 50-300 V, and setting the value of THL0 to 30 DAC units.

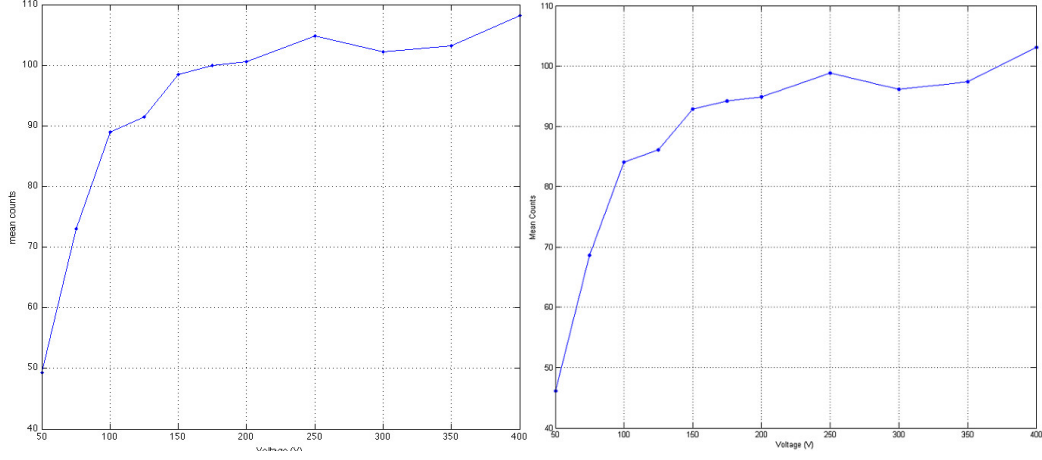


Figure 17: Left: Mean counts as a function of voltage. Right: Same, using only the inner part.

The average number of counts as a function of the bias voltage is shown in Fig.17 . There is a difference on the number of counts, with it being higher when taking into account the edge pixels, but the overall shape of the curves is the same.

The next table shows the mean value of counts as a function of voltage, as in Fig. 17, and also the standard deviations, taking into account all the pixels in the array.

Voltage (V)	Mean Counts	STD	Voltage (V)	Mean Counts	STD
50	49	7	200	101	10
75	73	8	250	105	10
100	89	9	300	102	10
125	91	9	350	103	10
150	98	10	400	108	10
175	100	10			

Table 3: Mean values and standard deviations for all bias voltages applied.

The mean counts are much lower than in the flat image analyzed before, shown in eq.1 , because now the noise is excluded by setting the THL0 higher. It can be easily seen that poissonian distribution condition shown before is still met.

2.3 Charge summing mode (CSM)

2.3.1 Flat images

As a first test for CSM, four sets of flat images are taken, with $t_{acq} = 0.1$ s and THL0=0. In each set, 100 images were taken and averaged. The X-ray tube is used with the same settings as before. The images were very similar with the four bias voltages used, so only one of them is shown (Fig. 18).

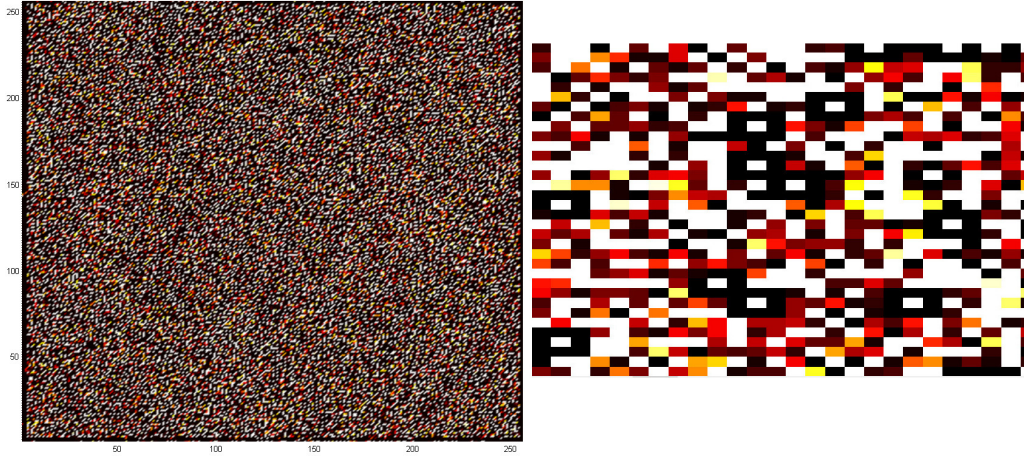


Figure 18: Flat image in CSM (300 V) and zoom.

The edge pixels are no longer saturated, with the edge being thinner than in SPM, about 3 pixels wide. In fact, most of them show zero counts. As shown in the zoom, a high amount of pixels are saturated (4095 counts, because 12-bit counters are being used) or show no counts at all. That is a consequence of photon hits being assigned to the wrong pixels because of different sensitivities of the summing nodes [1],[5]. This makes a non homogeneous image, radically different from the ones taken in SPM (for example, the persisting dark line seen in SPM is no longer visible), making CSM not suitable for imaging.

Table 4 shows the mean value and standard deviation for all four voltages applied.

Voltage (V)	Mean Counts	STD
50	1195	54
100	1184	54
200	1143	52
300	1118	49

Table 4: Mean values and standard deviations for all bias voltages applied. STD squared is no longer the same as the mean counts, so the Poissonian condition is not met anymore: the pixels seem to have larger variations than in SPM.

2.3.2 Response to different voltages

To compare the detector's response in SPM and CSM, THL scans are performed with the voltage values mentioned above, and are shown in Fig. 19. The region below $THL=40$ represents noisy counts, and the transition between noisy and non-noisy region is much more abrupt than before, which indicates that charge sharing effects are being corrected.

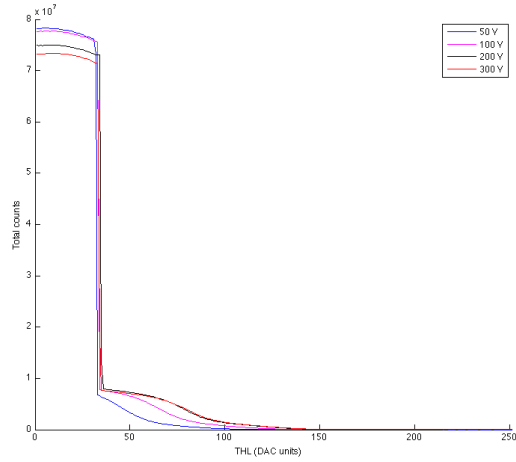


Figure 19: Threshold scans for all the bias voltages tested (total counts per step). Higher voltage settings make the detector more sensitive, as the curves show more counts around the molybdenum fluorescence energy, which is consistent with the results shown for SPM.

When the differentials of these curves are plotted in the region above noise (Fig. 20), the molybdenum fluorescence peak (around 18 keV) is easily seen.

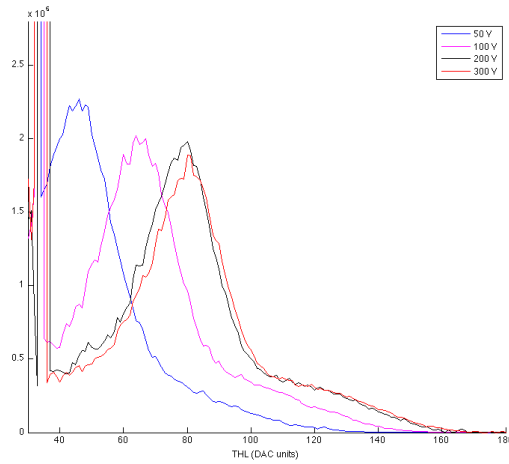


Figure 20: Zoom of the differential of the previous plots. The position of the peak is shifted when voltage is changed, possibly related to charge trapping effects, since the charge sharing effects are being compensated.

In conclusion, although CSM mode is worse for imaging, it is better for obtaining spectroscopic information. This can be used to calibrate the THL scale from digital units to energy. The voltage applied to the X-ray tube is 35 kV, in which case the maximum photon energy is 35 keV

. So, the fluorescence peak at 18 keV and the maximum energy at 35 keV correspond to digital values that can be obtained from the plots. To obtain the maximum photon energy, a linear fit is performed with the higher THL data, and its intersection with the x axis is the value that will be used. Those values and the conversion factors between DAC units and energy are shown in Table 5 for all four voltages. This cannot be accurately done in SPM.

Voltage (V)	Mo peak (DAC Unit)	Max energy (DAC Unit)	Conversion factors
50	46	127	1 DAC Step = 0.2099 KeV
100	64	143	1 DAC Step = 0.2152 KeV
200	80	160	1 DAC Step = 0.2125 KeV
300	80	163	1 DAC Step = 0.2048 KeV

Table 5: DAC-energy conversion. It is also worth noting that THL=0 does not correspond to zero energy.

2.3.3 Analysis for individual pixels

As done before, the response of individual pixels is worth studying, in this case, only the 300 V threshold scan is used. The pixels studied are the same ones as before (Fig.12 left, and Fig.16), which in SPM had average and very similar behaviours. The results in CSM are shown in Fig. 21 .

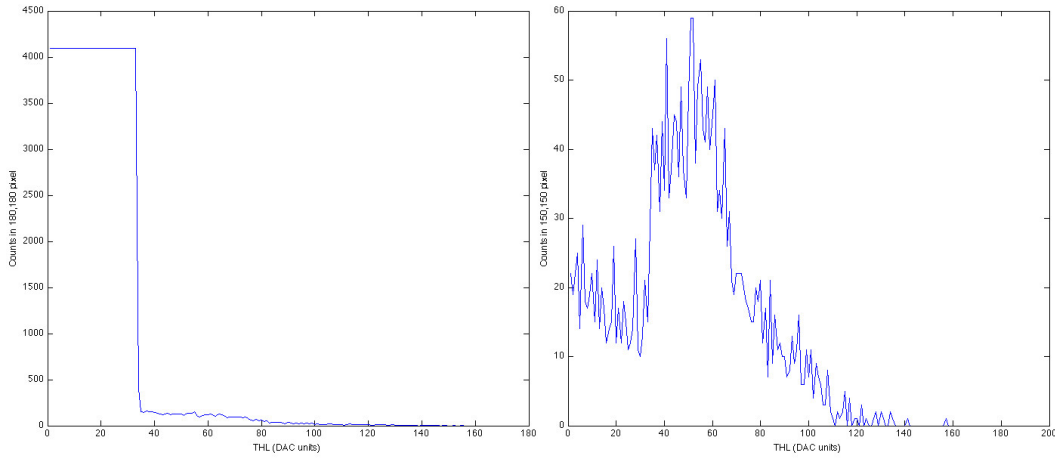


Figure 21: Left: the pixel keeps its normal response, same as in SPM. Right: the pixel is now dark, with a much lower amount of counts. These two pixels showed very similar plots in SPM, and show very different ones in CSM.

Also, the comparison between pixels with different sensitivities is performed again with the same ones (Fig.13 right).

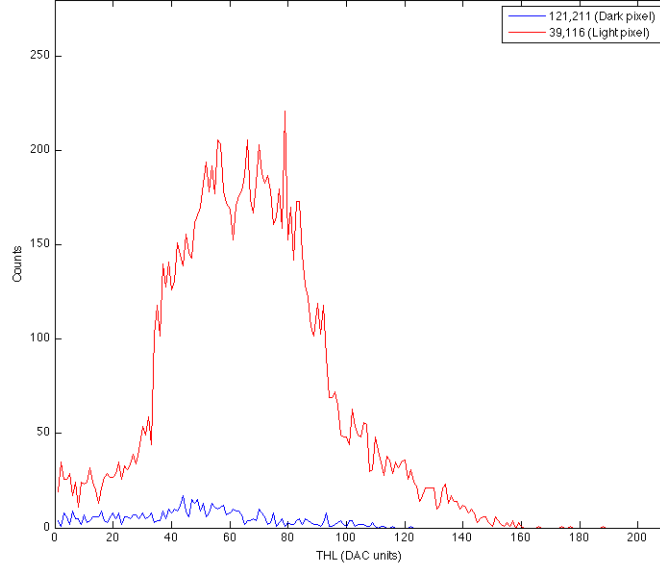


Figure 22: The differences both in shape and number of counts compared to SPM are obvious. Also, there is now a bigger difference between both pixels, one of them being almost dead.

2.3.4 Absorption Spectrum

Unlike SPM, CSM allows for spectral analysis. This makes some new measurements possible, such as absorption coefficients. In this case, several metal foils were placed in front of the detector, and the resulting spectrum measured through a THL scan, and also without any foil, for comparison. A total of four foils were used, made of brass, copper, aluminium and steel. The obtained spectra are shown in Fig. 23.

For monochromatic electromagnetic radiation, neglecting scattering effects, radiation intensity decays exponentially with penetration length d :

$$I = I_0 \cdot e^{-\mu d} \quad \ln\left(\frac{I_0}{I}\right) = \mu d$$

The total intensity is not needed, only the ratio between intensities both before and after the foil. To obtain it, gaussian fits are performed on the aluminium spectrum and on the source spectrum, around 18 keV, and the ratio of the maximum values is calculated. The values obtained from the fits are:

$$\text{Maximum}_{\text{no foil}} = (6.305 \pm 0.072) \cdot 10^5 \text{ counts}$$

$$\text{Maximum}_{\text{Al foil}} = (6.593 \pm 0.140) \cdot 10^4 \text{ counts}$$

This yields the value $\mu_{Al}d = 2.2579$.

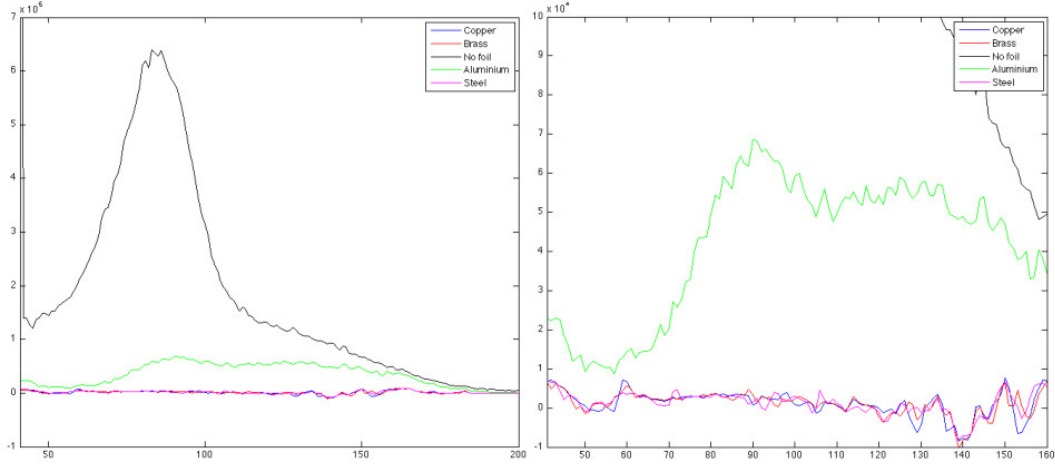


Figure 23: Spectra (differential of THL scans) with and without the foils. Only aluminium yields useful data

With that, and knowing the aluminium absorption coefficient for the used energy, the value obtained for the aluminium foil thickness is:

$$\mu_{Al}(17.8 \text{ keV}) \approx 12.5 \text{ cm}^{-1} \implies d \approx 1.8 \text{ mm}$$

3 Imaging

In this section, some images taken with the GaAs Medipix3 detector are shown. Also, they are compared with other images taken with two different silicon Medipix2 detectors with different thicknesses, namely $d = 300 \mu\text{m}$ and $d = 500 \mu\text{m}$. A 300 V bias voltage is applied in all cases. Prior to any acquisition a THL equalization must be performed. A threshold scan is also used to determine the adequate threshold level (THL0, THL for Medipix2) to leave out the noise. applied to the X-ray tube is 35 kV, in which case the maximum photon energy is 35 keV. So, the fluorescence peak at 18 keV and the maximum energy at 35 keV correspond to digital values that can be obtained from the plots. To obtain the maximum photon energy, a linear fit is performed with the higher THL data, and its intersection with the x axis is the value that will be used. Those values and the conversion factors between DAC units and energy are shown in Table 5 for all four voltages.

This cannot be accurately done in SPM.

The X-ray tube is set to are 40 kV and 40 mA. The bias voltage is set at 300 V in every case. It is worth noting that the silicon chips need the opposite polarity because of different doping. A total of 350 flat images with $t_{acq} = 0.2 \text{ s}$ are taken with each chip to perform a flat-field correction. It consists of multiplying each pixel's count value times a correction factor that contributes to minimize inter-pixel threshold differences or inhomogeneities in the source itself. To perform this, an average of the 350 images is calculated. Then, it is divided by its mean counts value, for normalization, and dark (less than a half of the mean) and too sensitive (more than 3/2 of the mean) pixels are not corrected. After that, all values are inverted and the array of correction factors is obtained. One example for this is shown in Fig. 24.

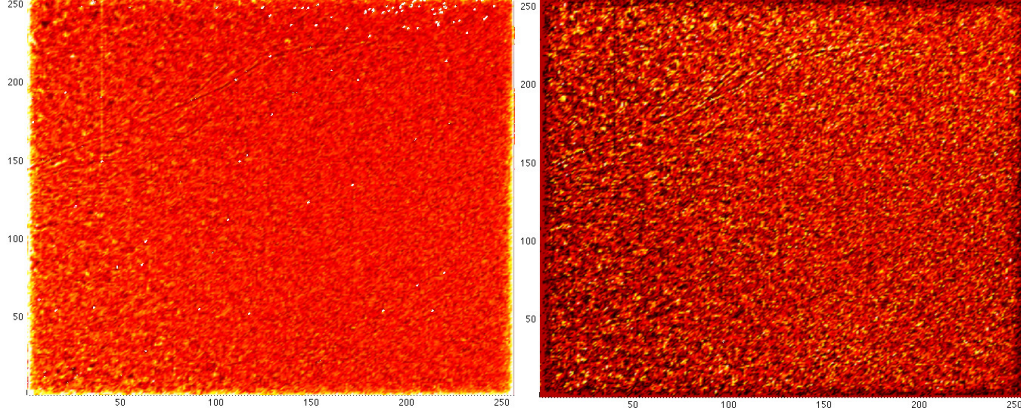


Figure 24: Flat image and correction factors for GaAs chip, $THL0=40$. The result is quite similar with $THL0=105$. In the case of both silicon chips (not shown), it is much more homogeneous, so the correction is not as important.

For comparisons to be made, raw and corrected images are presented with same colormap settings in each case.

3.1 Si Medipix2 chip, $300\ \mu\text{m}$ width

A threshold scan reveals that the optimal THL value is 350. The images taken with this chip are shown in Fig. 25, 26, 27.

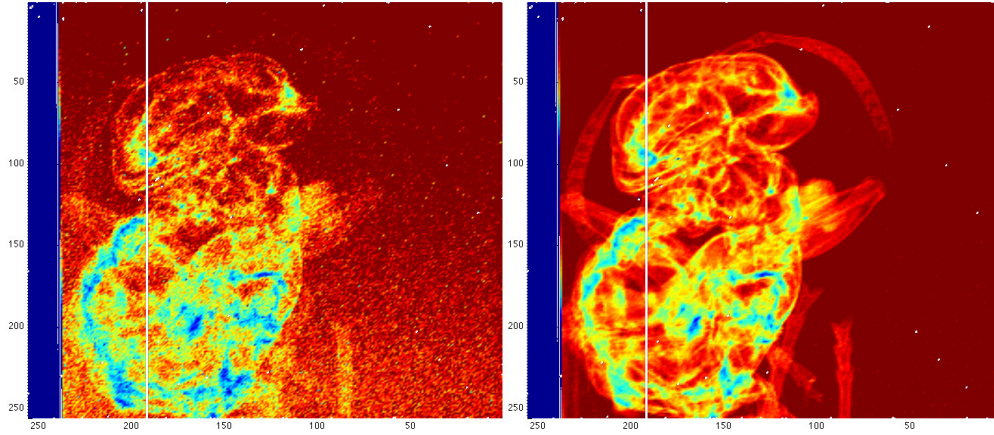


Figure 25: X-ray images of a hornet. Left, raw image. Right, corrected image. 1,000 images were taken with a 0.5 s acquisition time.

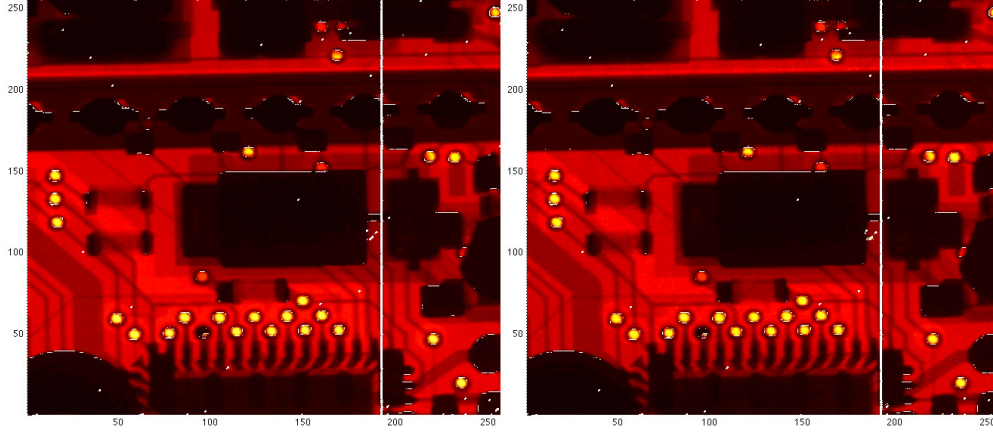


Figure 26: X-ray images of the Medipix interface. Left, raw image. Right, corrected image. 100 images were taken with a 1 s acquisition time.

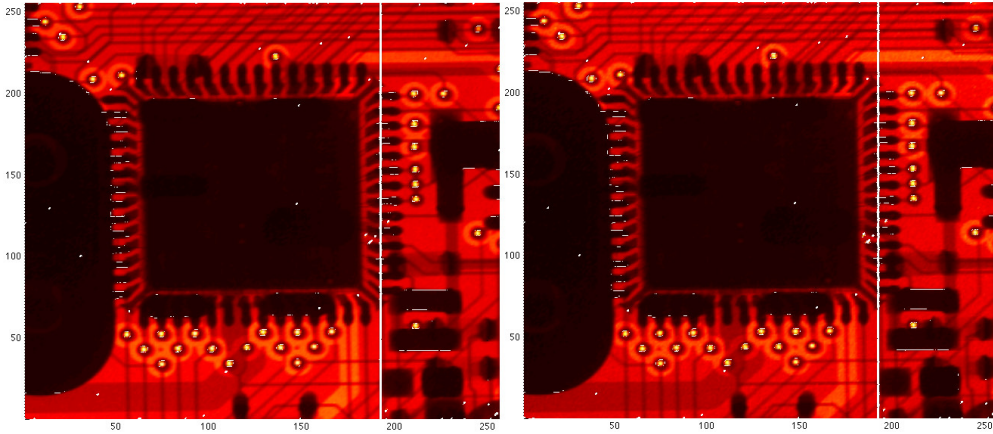


Figure 27: Same as Fig.26 from a different angle.

3.2 Si Medipix2 chip, 500 μm width

In this case, a THL value of 340 is used. The images are shown in Fig. 28, 29.

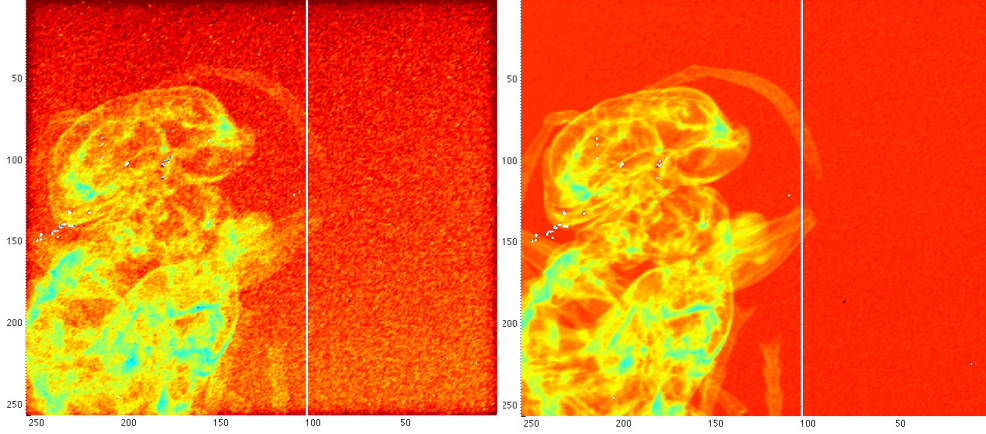


Figure 28: Raw and corrected X-ray images of the same hornet. 500 images with 1 s acquisition time.

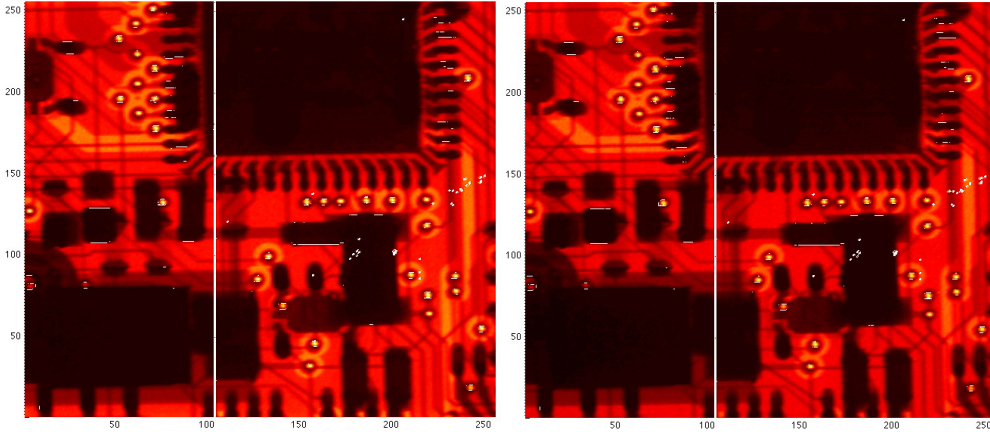


Figure 29: Raw and corrected images of the Medipix interface. 100 images with 1 s acquisition time.

3.3 GaAs Medipix3 chip

In this case, it is interesting to test the detector's response to higher energies. For that purpose, two different threshold levels are used. One of them leaves noise out, ($THL0=40$), and the other one leaves out the molybdenum fluorescence peak ($THL0=105$). Different flat-field correction factors must be obtained for each threshold. The resulting images are shown in Fig.30, 31, 32. The colormap for each threshold value is different, as the number of counts changes much with $THL0$. Also, only SPM is used, as CSM is not useful for imaging, as shown before.

The pixel-to-pixel variation is much larger in the GaAs than in silicon, which means that the raw images are poor, but the flat-field correction greatly improves the image.

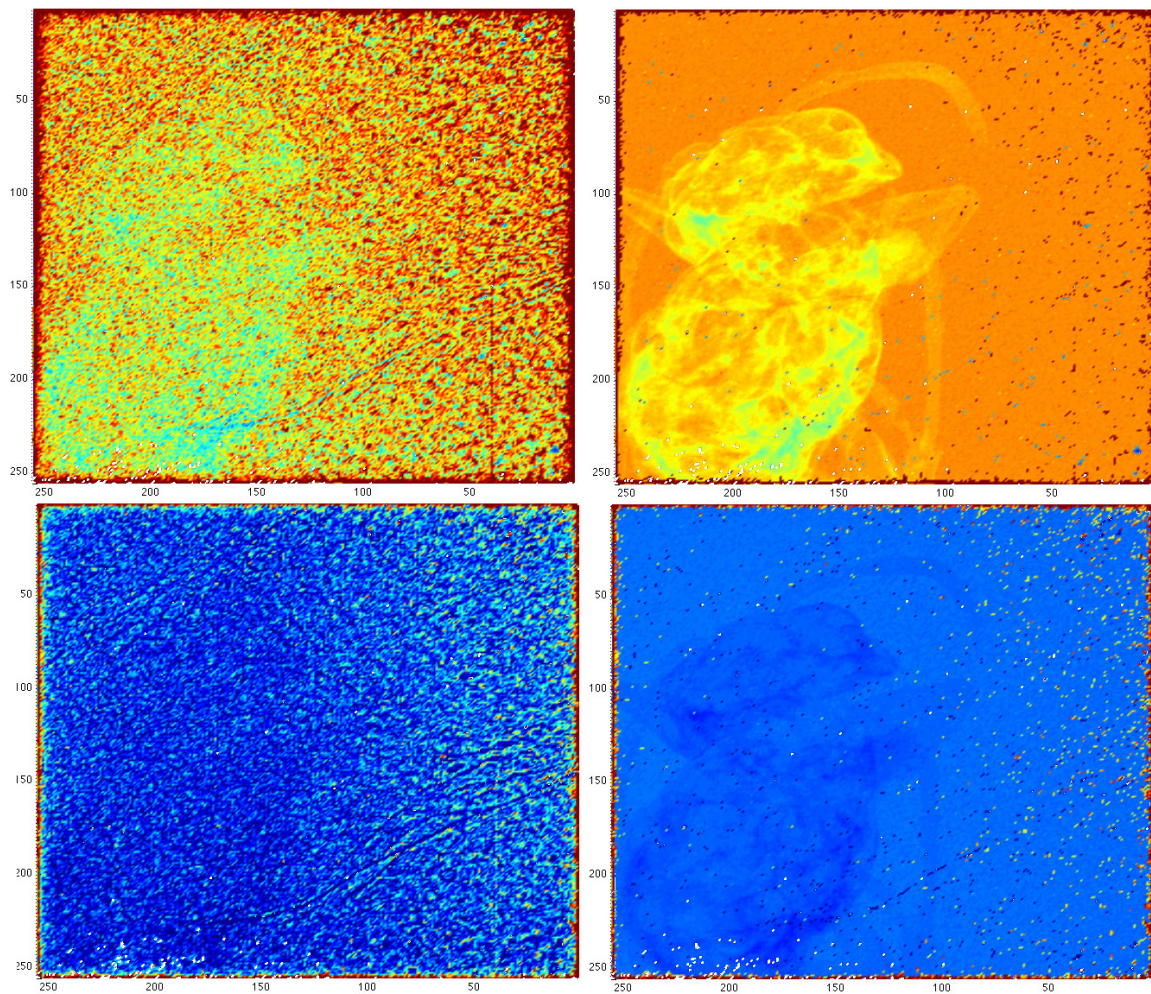


Figure 30: X-ray images of the hornet, both raw and corrected. Top, THL0=40, 500 images with 0.1 s acquisition time. Bottom, THL0=105, 500 images with 0.3 s acquisition time. The hornet becomes nearly transparent at higher energies. The flat-field correction is necessary in GaAs.

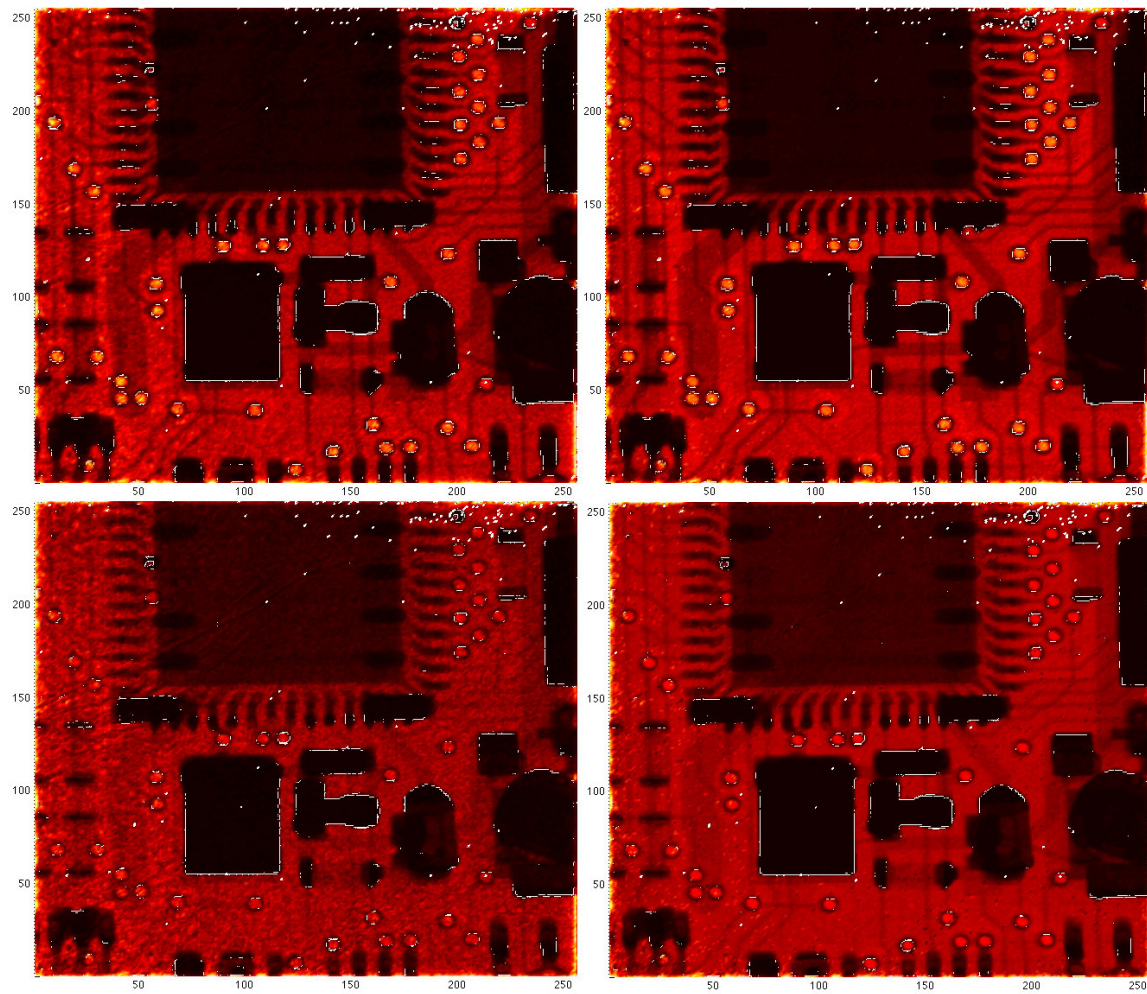


Figure 31: X-ray images of the Medipix interface, both raw and corrected. Top, THL0=40, 250 images with 0.4 s acquisition time. Bottom, THL0=105, 250 images with 0.4 s acquisition time.

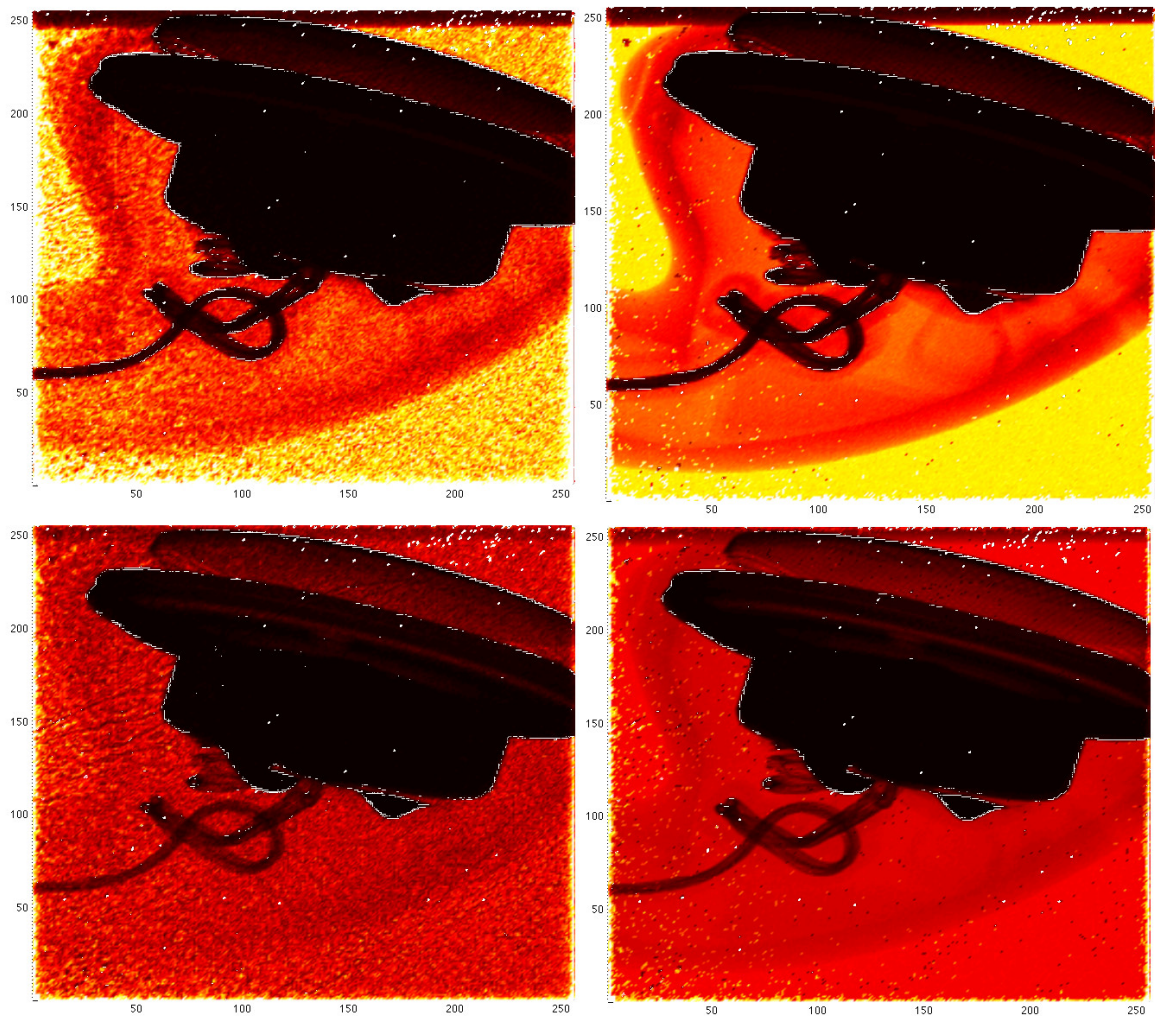


Figure 32: X-ray images of a earphone, both raw and corrected. Top, THL0=40, 500 images with 0.2 s acquisition time. Bottom, THL0=105, 250 images with 0.2 s acquisition time.

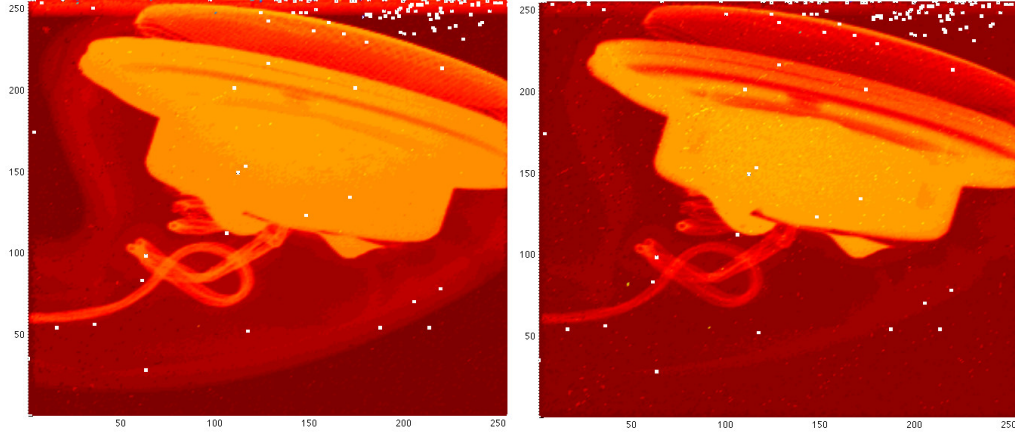


Figure 33: Same X-ray images in logarithmic scale. Left, $THL0=40$. Right, $THL0=105$. Some more details are revealed in the metallic structure.

4 Conclusions

Several tests were performed with a GaAs Medipix3 chip. Several conclusions about its response can be drawn from the obtained results:

The optimal bias voltage for the GaAs chip is in the range between 200 and 300 V, with negative polarity.

Both SPM and CSM were tested, and show different properties. Whereas SPM is good for imaging purposes, it does not show realistic spectroscopic information due to charge sharing effects.

CSM shows exactly the opposite properties: it is not suitable for imaging due to counts not being assigned to the correct pixels, and allows for good spectroscopy-related measurements, such as absorption coefficients.

Also, the GaAs detector performs well for imaging purposes with high-energy photons (between 20 and 40 keV, in this work).

References

- [1] D. Pennicard , R. Ballabriga, X. Llopart, M: Campbell, H. Graafsma. “Simulation of charge summing and threshold dispersion effects in Medipix3”. Nucl. Instr. and Meth. A 636 (2011) 74.
- [2] R. Ballabriga, M. Campbell, E. Heijne, X. Llopart n, L. Tlustos, W. Wong. “Medipix3:A 64k pixel detector readout chip working in single photon counting mode with improved spectrometric performance”. Nucl. Instr. and Meth. A 633 (2011) S15.
- [3] D. Pennicard. “3D Detectors for Synchrotron Applications”. PHD thesis (2009) University of Glasgow.
- [4] T. Dobbelaere. “Testing the Medipix3 photon-counting detector”. Report for the Summer Student Program, Desy (2011).
- [5] E. N. Gimenez, R. Ballabriga, M. Campbell, I. Horswell, X. Llopart, J. Marchal, K. J. S. Sawhney, N. Tartoni, D. Turecek. “Characterization of Medipix3 with Synchrotron Radiation”. IEEE Trans. Nucl. Sci. 58 (1) , February 2011, 323-332.